

Temperature Dosimetry Using MR Relaxation Characteristics of Poly(vinyl Alcohol) Cryogel (PVA-C)

L.A. Lukas, K.J.M. Surry, and T.M. Peters*

Hyperthermic therapy is being used for a variety of medical treatments, such as tumor ablation and the enhancement of radiation therapy. Research in this area requires a tool to record the temperature distribution created by a heat source, similar to the dosimetry gels used in radiation therapy to record dose distribution. Poly(vinyl alcohol) cryogel (PVA-C) is presented as a material capable of recording temperature distributions between 45 and 70°C, with less than a 1°C error. An approximately linear, positive relationship between MR relaxation times and applied temperature is demonstrated, with a maximum of 16.3 ms/°C change in T_1 and 10.2 ms/°C in T_2 for a typical PVA-C gel. Applied heat reduces the amount of cross-linking in PVA-C, which is responsible for a predictable change in T_1 and T_2 times. Temperature distributions in PVA-C volumes may be determined by matching MR relaxation times across the volumes to calibration values produced in samples subjected to known temperatures. Factors such as thermotolerance, perfusion effects, and thermal conductivity of PVA-C are addressed for potentially extending this method to modeling thermal doses in tissue. *Magn Reson Med* 46:1006–1013, 2001. © 2001 Wiley-Liss, Inc.

Key words: poly(vinyl alcohol) cryogel; temperature dosimetry; MR relaxation; phantoms

Advances in source-applied medical treatments have demanded more accurate planning and targeting techniques, which has driven research in dosimetry test models. For conformal radiotherapy, dosimetric gels have been prevalent in the literature as an appropriate tissue model for radiation planning (1–5). Three-dimensional information can be directly acquired from an irradiated gel through optical tomographic scanning or MRI. This is an improvement on the previous mode of planning, in which doses were recorded with 2D films.

Applied heat, or hyperthermic therapy, is being used for a variety of medical treatments, including the enhancement of radiation treatment, direct tumor ablation, or for the creation of therapeutic lesions in the treatment of parkinsonian tremor and epilepsy (6,7). Currently, however, there is no means analogous to a radiation dosimetry gel for recording the 3D temperature distribution generated by an applied heat source.

Tissue heating may be applied through RF probes, lasers, microwaves, or high-frequency ultrasound (6,8). Low-temperature hyperthermia in the range of 43–45°C is used in applications such as radiation therapy to kill cancer cells or to improve the tissue's response to applied

radiation (7–9). High-temperature hyperthermia, where temperatures range from 50–80°C, causes protein denaturation and subsequent tissue necrosis (9). To cause permanent damage, or cell death, for therapeutic lesioning, the temperature must be above 45°C, while temperatures between 42–44°C will cause temporary, reversible cell damage (6). Thus, to create therapeutic lesions the temperature in the target tissue must be raised above 45°C, causing a surrounding fall-off region of temporary damage. The two goals of therapeutic lesioning are, first, to ensure that the targeted volume of tissue has been adequately heated to cause necrosis, while minimizing the amount of surrounding tissue exposed to critical temperatures and irreversible damage (9).

Studies have been performed to monitor heating processes in real time, including using thermocouples during the heat treatment of wounds (9), and in vivo monitoring in MRI of applied radiotherapy (9–20). MR thermometric methods, such as proton-resonance frequency (PRF) shift (9,12,16,18–20), spin-lattice relaxation time (13–20), and diffusion coefficient of water (13,15–16,18–20) are real-time procedures that provide a minimally invasive measurement of temperatures induced in tissue samples or phantoms. PRF appears to be the most reliable method for temperature estimation due to its linear behavior and ease of measurement, and because its thermal coefficient (usually reported as the PRF change in ppm/°C) is similar for many tissue types (9,16). Although there are concerns about irreversible behavior between heating and cooling, difficulty of measurement and interpretation, and a need for a priori thermal calibrations for each of the MR thermometry methods (9), the temperature sensitivities are generally within 1°C, with an accuracy of 0.37°C being reported by de Zwart et al. (21).

These thermometry methods are limited to real-time imaging, but there are advantages to having a tool that would maintain a permanent postheating thermal record in three dimensions in order to study the heat distribution mechanisms of surgical probes. Our objective in this work was to develop a way to determine the shape of a heat-affected region caused by an RF probe. This is particularly important when developing RF probes that create lesions with shapes other than the isotropic ellipsoid created by standard probes.

Theoretical models have been proposed as predictive tools for lesion planning and have been supported by postoperative MR images of heat-created lesions (8,22). However, comparison with a high-resolution experimental model, which provides heat gradients in three dimensions, would provide a more robust model that would also detail the extent of reversible tissue damage. This experimental model would be similar in function to radiation dosimetry

Imaging Research Laboratories, The John P. Robarts Research Institute, Department of Medical Biophysics, University of Western Ontario, London, Ontario, Canada.

Grant sponsor: Canadian Institutes of Health Research; Grant numbers: MOP-14735; MT-11540.

*Correspondence to: Dr. Terry Peters, The John P. Robarts Research Institute, PO Box 5015, 100 Perth Drive, London, Ontario N6A 5K8, Canada. E-mail: tpeter@irus.ri.on.ca

Received 22 August 2000; revised 16 May 2001; accepted 5 June 2001.

gels and would record thermal dose, which would then be quantified postheating.

We present poly(vinyl alcohol) cryogel (PVA-C) as a suitable candidate for thermal dosimetry. Through previous work we have done in creating PVA-C phantoms for medical imaging studies (23,24), it was apparent that this material's structure is sensitive to temperature application, at least in its formation process. We believe that this temperature sensitivity could be extended to the controlled heating of the cryogel after gelation and it was hypothesized that the MR imaging characteristics of PVA-C could be related to the temperature distribution caused by the hyperthermic therapy.

Poly(vinyl alcohol) cryogel is a nontoxic, elastic, mechanically strong gel, whose properties make it particularly suitable for the construction of medical imaging phantoms (23–25). PVA-C was first developed by Mano et al. (26), who devised a method of repeatedly freezing and thawing a uniform, highly hydrolyzed PVA solution into a medium called Nambu Poly(vinyl alcohol) gel, which has elastic properties similar to those of many human tissues. This cryogel solidifies during the freeze-thaw process as hydrogen bonds form between water and the hydroxyl groups on the PVA molecules (27). A higher concentration of the PVA molecule in water causes a higher degree of hydrogen bonding, which contributes to an increased elastic modulus of the cryogel. Likewise, as the number of freeze-thaw cycles (FTCs) increases the degree of hydrogen bonding also increases and contributes to the elastic modulus (27). Finally, the rate of thaw can also affect the elastic modulus, as slow thaw rates have been shown to increase the amount of PVA cross-linking (23).

PVA-C has been successfully used to mimic organs and tissues in imaging phantom studies. This material exhibits close to ideal imaging and mechanical properties and these can be prescribed to some extent (23,24). The factors that affect the material characteristics are PVA-C concentration, number of FTCs, thawing rates, additives (echogenic particles and preservatives) (23), and, as discussed below, exposure to a heat source.

MATERIALS AND METHODS

Sample Preparation

Two types of PVA solutions were prepared: 10% PVA by weight in water and another 15% by weight. A syringe was used to transfer 1 mL of PVA solution into 5 mL cuvettes ($1 \times 1 \times 5$ cm). The samples were placed in a freezer in which the temperature was slowly decreased from ambient to -20°C in a 12 h freezing stage. The resulting characteristics of the cryogel have been shown to be independent of the freezing rate (28).

The effect of different concentrations, FTCs, and thaw rates were evaluated through different preparation protocols for the PVA cuvette samples. Twenty cuvettes of 10% solution were subjected to one freezing stage, then thawed in room-temperature water. Another subset of 20 cuvettes of 10% solution and a set of 15% PVA cuvettes were subjected to one freezing stage, then thawed slowly in the freezer from -20°C to $+20^{\circ}\text{C}$ within a 6 h period, at approximately $7^{\circ}\text{C}/\text{h}$. This is a typical FTC. A third set of

20 cuvettes of 10% solution were subjected to a second FTC.

Three sets of 60 PVA-C samples were prepared in this manner, so that three heating trials could be conducted to assess repeatability and stability.

Twenty-five additional cuvettes of 10% PVA-C, with two FTCs, were prepared to explore the thermal behavior of PVA-C.

Two circular cylinders, 5 cm in diameter and 12 cm long, of 10% 2FTC PVA-C, were made for the gradient mapping and thermal conductivity studies. These phantoms were formed with a central cylindrical void, made from a plastic rod inserted into the PVA during the FTCs.

Sample Heating

A water bath was used to heat the samples. Nineteen samples from each heating trial subgroup were heated in intervals of 2°C for a temperature range of 36 – 72°C . The twentieth samples from each series were kept as controls. Each 5 min heating period was terminated by temporarily immersing the samples in room-temperature water.

The samples of PVA-C were heated sufficiently to ensure that a uniform temperature had been achieved. After 5 min of heating at any temperature between 36 – 72°C , the samples were visibly uniform in their translucency. This steady state was confirmed through uniformity in MR relaxation times across the cross-section of each sample.

To explore the effect of thermal history on PVA-C, the other 25 prepared cuvettes were used. Five of these were kept as controls and were not heated. The next set of five cuvettes was heated to 60°C in the water bath and cooled rapidly to 20°C in a cold bath. This heating pattern was applied twice to a third set of five cuvettes. The fourth set of five was heated to 60°C , cooled to 20°C , heated to a different peak temperature of 50°C , and cooled to 20°C . The final set of five cuvettes was heated first to 50°C , cooled to 20°C , and then heated to 60°C before being cooled back to 20°C .

MR Relaxation Times

After heating, the samples were bundled together and imaged in a GE Signa 1.5T MRI. Imaging was performed within 10 h of heating to minimize any potential decay of temperature memory with time. Local image signal-to-noise was improved through the use of an extremity gradient coil in the last two of the three heating series trials and the thermal history trial. Image quality was also improved by having the samples close together and in a water bath. The close proximity of the samples allowed them to fit inside a small gradient coil and the water served to minimize susceptibility-induced edge effects. Two weeks later, the samples from the third heating series trial were reimaged to assess the longer-term stability of the heated PVA-C in both T_1 and T_2 .

The T_1 relaxation times were acquired using a 2D-inversion recovery (IR) sequence. The inversion time (TI) was varied for seven acquisitions (Fig. 1) using the following scanning parameters: variable bandwidth, extended dynamic range, 3 mm thick slice, single slice, 256×192 matrix, 1 NEX, 0.75 phase FOV, S/I frequency direc-

tion, one echo, TR = 5000 ms, TE = 14.0 ms, and TI = 50, 100, 200, 400, 800, 1600, and 3200 ms, in sequence.

The T_2 relaxation times were obtained using a 2D-spin echo sequence (Fig. 2) with the following parameters: variable bandwidth, extended dynamic range, 3 mm thick slice, single slice, 256×192 matrix, 1 NEX, 0.75 phase FOV, S/I frequency direction, one echo, TR = 5000 ms, and TE = 20, 40, 80, 160, 320, 640, and 1280 ms, in sequence.

Analysis

The data acquired from the 2D-IR images were fitted to the standard signal intensity equation (Eq. [1]) using custom-written MATLAB scripts (MathWorks, Natick, MA). A cross-sectional region of interest (ROI) was manually selected in one of the seven IR series images for each of the PVA-C samples. Using the average signal intensity values calculated in each of the seven images for that ROI, a curve was plotted against the range of TI values and T_1 was determined.

$$SI = S_o(1 - 2e^{-TI/T_1} + e^{-TR/T_1}) \quad [1a]$$

Since $TR \gg T_1$, Eq. [1a] may be rewritten as:

$$SI = S_o(1 - 2e^{-TI/T_1}) \quad [1b]$$

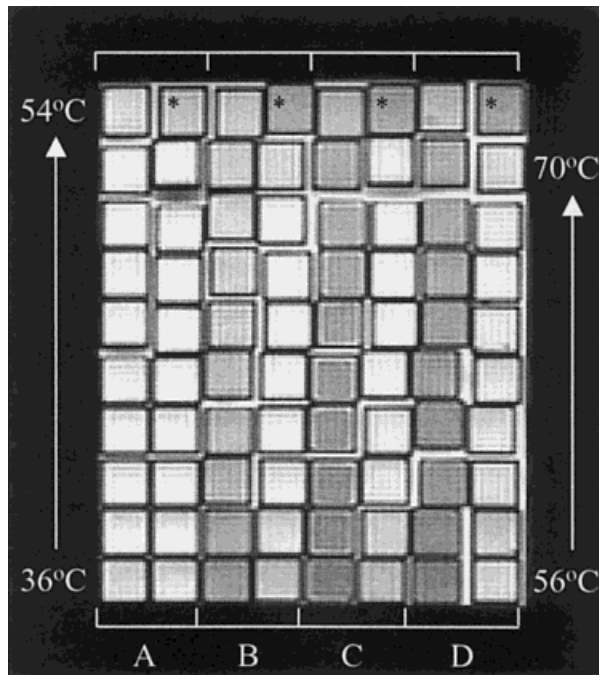


FIG. 1. An inversion recovery image of the PVA-C samples, from the series of images obtained to find T_1 values. From the left, each series consists of two columns of cuvettes: **A**: 10% 1FTC quick-thaw, **B**: 10% 1FTC, **C**: 10% 2FTC, **D**: 15% 1FTC. From bottom to top, the samples were heated with increasing temperature, as indicated. The final cuvette in each series, marked with an asterisk (*), is the control sample.

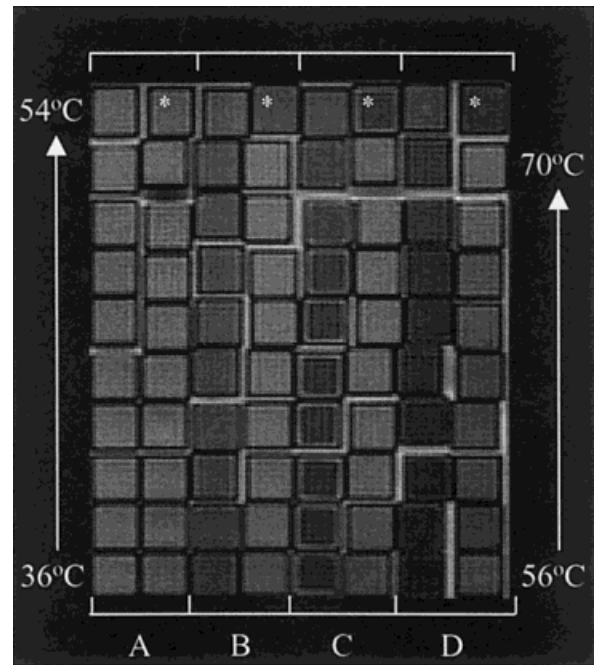


FIG. 2. A spin echo image of the PVA-C samples, from the series of images obtained to find T_2 values. From the left, each series consists of two columns of cuvettes: **A**: 10% 1FTC quick-thaw, **B**: 10% 1FTC, **C**: 10% 2FTC, **D**: 15% 1FTC. From bottom to top, the samples were heated with increasing temperature, as indicated. The final cuvette in each series, marked with an asterisk (*), is the control sample.

SI is the signal intensity of the selected ROI of the image and S_o is equal to $-SI$ at a TI value of zero.

Likewise, the data acquired from the 2D-spin echo sequence images were fitted to Eq. [2]:

$$SI = S_o(1 - e^{-TR/T_1})e^{-TE/T_2} \quad [2a]$$

Since $TR \gg T_1$, Eq. [2a] may be rewritten as:

$$SI = S_o e^{-TE/T_2} \quad [2b]$$

SI is the signal intensity of the selected ROI and S_o is SI at a TE value of zero.

The T_1 and T_2 values were then plotted against the temperatures corresponding to the heating series samples for which they were calculated, and this set of data was represented by a least-squares fit. T_1 and T_2 values were also obtained for the PVA-C samples subjected to thermal cycling.

Gradient Mapping

A preliminary study was conducted to look at the heat distribution in a cylindrical sample of PVA-C. The gradient was created by submerging the 5 cm diameter sample of 10% 2FTC PVA-C into a controlled 70°C water bath until the PVA-C's internal temperature reached 50°C (measured at approximately 1.5 cm from the cylinder's edge). A 1.2 cm diameter aluminum rod inserted into the center of the PVA-C cylinder served as a heat sink. Upon removal,

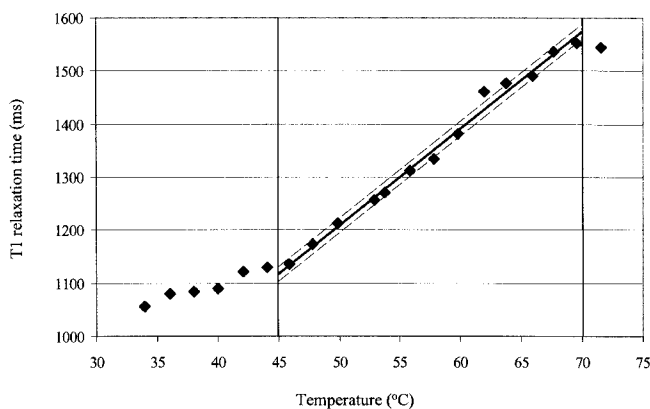


FIG. 3. Mean T_1 values, plotted against temperature, for 10% 2FTC PVA-C. The linear section between 45 and 70°C is indicated. In this region a line of best fit is also plotted and the error range is shown by dashed lines.

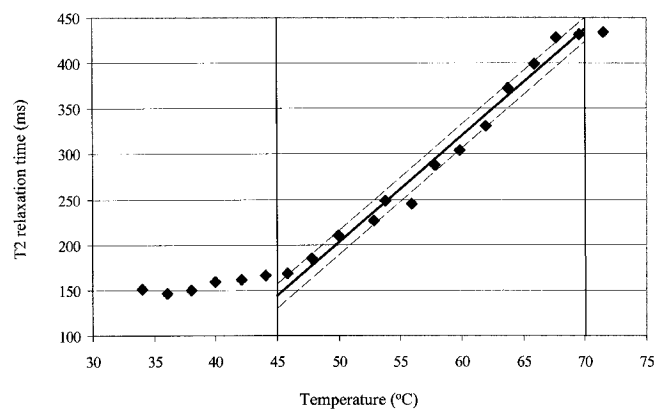


FIG. 4. Mean T_2 values, plotted against temperature, for 10% 2FTC PVA-C. The linear section between 45 and 70°C is indicated. In this region a line of best fit is also plotted and the error range is shown by dashed lines.

the cylinder was immersed in a cool water bath to halt further heating. Images were acquired using the inversion recovery sequence, with the same parameters as the initial experiments, to obtain the 2D T_1 relaxation map. A profile of the relaxation gradient was obtained by averaging the pixel values of the T_1 map at each radial distance of the cylinder cross-section.

Thermal Conductivity

To determine the thermal conductivity of 10% 2FTC PVA-C using the methodology outlined by Touloukian et al. (29) for radial heat flow, the heat flow through a 5 cm diameter aluminum cylinder with known thermal conductivity was compared to the heat flow through an identical cylinder of 10% 2FTC PVA-C. Thermocouples were inserted at radii of 5 mm and 15 mm from the outer edges of the cylinders and the time-dependent temperatures were recorded over a 150 sec time interval in a 70°C water bath.

RESULTS AND DISCUSSION

Temperature Prediction

There was an increase in relaxation time with temperature in all cases. The curves showing the relationship between temperature and T_1 and T_2 times are shown for 10% 2FTC PVA-C in Figs. 3 and 4, respectively. The relaxation times are approximately linear with temperature over the range 45–70°C and there is a noticeable leveling off of the values outside this range. At the lower end, this may indicate that

the added heat was not yet sufficient to affect the PVA-C and its corresponding relaxation times. At the upper end of the temperature scale, an equilibrium point may have been reached where the PVA-C was thoroughly melted and thus all the relaxation times for temperatures above this point would be the same. The positive linear relationships in the temperature range of 45–70°C are also shown in Figs. 3 and 4. This demonstrates the capacity for temperature memory in 10% 2FTC PVA-C. We suggest that the temperature memory can be attributed to the breaking of the hydrogen bonds through the application of heat. By this mechanism, changes in the structure of the PVA-C are reflected in elevated T_1 and T_2 relaxation times as the cryogel moves to a more liquid state. Since the melting point of the PVA molecules is much greater than 70°C (about 200°C), the changes are not attributable to bonding disruptions in the PVA polymer itself.

The linear correlation between relaxation times and temperature improved with increased concentration, increased number of FTCs, and a prolonged thawing period (Table 1). The 10% 2FTC samples possessed the largest change in relaxation time with temperature, 16.3 ms/°C for T_1 and 10.2 ms/°C for T_2 . All PVA-C types produced curves with an inexplicable, nonlinear ‘bump’ at 52–56°C, but this effect is minimal in the 10% 2FTC samples and this is reflected in the R^2 values. Without further investigation of this characteristic, only 10% 2FTC PVA-C can be recommended as the most linear curve and T_1 as providing a more reliably linear relationship than T_2 (R^2 values of 0.99 and 0.98 for T_1 and T_2 fits, respectively; see Table 1).

Table 1
Correlation Coefficients, Relaxation Time Ranges, and Temperature Errors for T_1 and T_2 , Over a Temperature Range of 45–70°C

		10% 1FTC quick-thaw	10% 1FTC	15% 1FTC	10% 2FTC
T_1	R^2	0.8993	0.9655	0.9876	0.9905
	T_1 range (ms)	156	322	271	423
	Temperature error (°C)	±2.9	±1.6	±1.0	±0.8
T_2	R^2	0.8116	0.9776	0.9757	0.9757
	T_2 range (ms)	197	263	175	265
	Temperature error (°C)	±4.1	±1.3	±1.4	±1.4

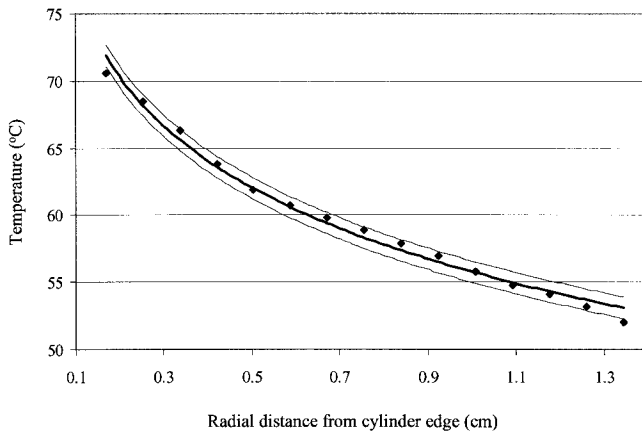


FIG. 5. Temperature gradient in a cylinder of 10% 2FTC PVA-C, derived from T_1 values. The line of best fit is plotted and the error range is shown.

The standard error was calculated for each PVA-C type to relate a given T_1 or T_2 value to a temperature lying within its calculated error range. The error range was reduced with an increase in concentration, number of FTCs, and thawing time (Table 1). The 10% 2FTC samples contained the least error, making it possible to match a given T_1 relaxation time to the temperature previously applied to a sample of 10% 2FTC PVA-C accurate to $\pm 0.8^\circ\text{C}$, in the range of $45\text{--}70^\circ\text{C}$ (Fig. 3). This standardized temperature gradient scale could be used to determine an unknown temperature applied to a sample of PVA-C by matching the T_1 and T_2 values of an imaged sample to their corresponding temperatures. Using Eq. [3], the temperature, t , of a pixel or region in the image can be found from its T_1 ([3a]) or T_2 ([3b]) value:

$$t = 0.555T_1 - 16.10$$

$$R^2 = 0.99 \quad [3a]$$

$$t = 0.085T_2 + 32.73$$

$$R^2 = 0.98. \quad [3b]$$

To investigate this procedure, the T_1 map of the cylindrical PVA-C gradient sample was used. The T_1 values were averaged for 15 cylinder radii and were used in Eq. [3a] to plot the temperature gradient (Fig. 5). The logarithmic trend follows the form for a steady-state heat conduction model for a cylinder (30):

$$t = t_o - \frac{q}{2\pi kL} \ln\left(\frac{r}{r_o}\right). \quad [4]$$

Here, q is the heat conduction rate in the radial direction (in $\text{Js}^{-1}\text{m}^{-1}$); k is the thermal conductivity of the material (in $\text{Wm}^{-1}\text{K}^{-1}$); L is the length of the cylinder (in m); r is the relative radial position from the center of the cylinder (in m); r_o is the radius of the cylinder (in m); t is the temperature at position r (in K); and t_o is the temperature at the outer edge of the cylinder (in K) (30).

The curve of best fit to the data shown in Fig. 5 is:

$$t = -7.11 \ln(r) + 72.90$$

$$R^2 = 0.97. \quad [5]$$

The analysis assumes a steady-state situation. This is a simplification of the heat transfer mechanism, as it assumes that there is a perfect heat sink in the center of the cylinder. Without such a heat sink, a nonsteady-state analysis is more accurate. With only this single proof-of-concept case, a full analysis was unwarranted and the good fit ($\chi^2_{0.05}$) to the form of the steady-state model provides enough confirmation that this method is working sufficiently well to predict temperature gradients in PVA-C.

The T_1 and T_2 imaging methods used above are known to be approximate; a 'pure' CPMG sequence was not available, so a single-echo spin echo sequence with incremented echo times was used to find T_2 . Repeatability of measurements is more important here than accuracy. With a repeatable technique, uncontrolled heating patterns can be analyzed using results from controlled heating studies, as long as the preparation of the phantoms and the acquisition of data is kept the same. The scales given here for relaxation time to temperature are not meant to be absolute, but instead are a demonstration of the capability to make a reference scale for any given condition. The actual relationship between relaxation time and temperature will depend on the precise parameters used to manufacture the PVA-C.

Statistical Analysis

T -tests were used to analyze the effects of concentration, number of FTCs, and thawing rate on the T_1 and T_2 changes with increasing temperature.

Significant differences ($P < 0.01$) were found between the relaxation times for the 10% PVA-C samples and the 15% PVA-C samples, as well as for PVA-C prepared by quick thaw, 1FTC and 2FTC. These findings are consistent with the descriptions of the mechanisms affecting hydrogen bonding given by Nagura et al. (27) and Mori et al. (28).

The results of the three independent heating trials demonstrated the reproducibility of the T_1 and T_2 relaxation times for the temperature range. Significant differences were not found between the relaxation times of each series type compared from one trial to the next, except in three anomalous cases. These differences in T_1 relaxation times may be due to experimental error, since they were not consistently found in a particular series-type when comparing the three trials.

After 2 weeks, the samples from the third trial were imaged again to assess the longer-term stability of the heated PVA-C's MR characteristics. For the series with equal variances, analysis with repeated-measures t -tests ($\alpha = 0.05$) showed significant differences between the initial values and the reimaged T_2 values for the quick thaw and the 10% 1FTC samples, but no significant differences for the T_2 values of the 10% 2FTCs series or the T_1 of the 15% 1FTC series. For the series with unequal variances, a Wilcoxon Signed Rank Test for the Paired Difference Experiment ($\alpha = 0.05$) showed significant differences

between the initial values and the reimaged T_1 values for the quick-thaw and the 10% 1FTC series, but no significant differences for the T_1 values of the 10% 2FTCs series or the T_2 values of the 15% 1FTC series. To summarize, the relaxation characteristics of the 10% 2FTCs and the 15% 1FTC series were stable after a period of 2 weeks.

Thermal History

The PVA-C cuvettes which were subjected to two peak temperatures (as described above) provided an indication of peak temperatures when the samples were heated to steady state. Using an ANOVA analysis, no hysteresis was evident from cycling the system twice between its minimum and maximum temperatures. That is, the relaxation values for the highest peak temperatures were not significantly different from those of the cuvettes subjected to only one heating cycle ($\alpha = 0.05$), except when the order of the peak temperatures was reversed. With maximum temperatures of first 50°C and then 60°C, the T_2 values indicated no significant difference from the other samples heated to 60°C, but the T_1 values indicated a slightly lower relaxation value ($\alpha = 0.05$). Further study is necessary to examine the cause of the discrepancy.

Thermal Conductivity

It was demonstrated that the thermal conductivity may be determined by comparison of the radial heat flow through an aluminum cylinder with known thermal conductivity and an identical cylinder of 10% 2FTC PVA-C. After 80 sec of heating the PVA-C cylinder, the inner thermocouple (at 15 mm) recorded a temperature increase and the heating was stopped. The thermocouple readings for the two points in each of the PVA-C and the aluminum cylinders were used to estimate the thermal coefficient for this sample of PVA-C. Using the temperature readings and the thermal conductivity coefficient for aluminum ($k_{Al} = 240 \text{ Wm}^{-1}\text{K}^{-1}$) (42) in Eq. [4], the heat conduction rate, q , could be estimated and used again in Eq. [4] to further estimate k_{PVA-C} . This was found to be $6.5 \text{ Wm}^{-1}\text{K}^{-1}$. Literature values for brain tissue thermal conductivity range from 0.4–0.6 $\text{Wm}^{-1}\text{K}^{-1}$ (43).

Applications

The initial motive for using PVA-C in thermal dosimetry was to validate theoretical models of the temperature distribution from an RF probe. To avoid artifacts associated with the metallic probes, we decided against using real-time dynamic methods such as proton resonance frequency shift MRI. Although PVA-C has been shown to record thermal dose through predictable changes in its T_1 and T_2 values, the study up to this point has concentrated solely on assessing the MRI characteristics of heated PVA-C and has not yet been extended to using PVA-C as a predictor of lesion size in tissue from an RF heat source.

Factors would need to be considered to extend this technique to modeling the effect of heat deposition in tissue, including the thermal conductivity of PVA-C in relation to that of tissue, and the complex response of tissue to hyperthermia, with respect to its thermotolerance (16,31–35). Thermal ablation is influenced by intrinsic cell

or tissue susceptibility, spatial distribution of temperature, duration of heating, rate of heating, pH levels (32), but perhaps most importantly, the convective heat loss due to local perfusion (36–38). As pointed out by Jain and Wolf (37), the models of thermal ablation by Labonte (39), Shahidi and Savard (40), and Panescu et al. (41) do not take into account the electrical conductivity of tissue or blood. However, Haines and Watson's study (38) of the RF catheter ablation in canine right ventricular free wall, the lesion depths, widths, and volumes were independent of intramyocardial perfusion when a constant electrode tip temperature was maintained. Likewise, the measured difference in the amount of energy maintaining the constant tip temperature in the flow vs. nonflow states was negligible (38). According to Haines and Watson (38), this phenomenon could be caused by coagulation of the microvasculature, heat-induced vasoconstriction causing a decrease in local intramyocardial perfusion while maintaining the total epicardial perfusion, or because the arteriolar and venular blood are thermally coupled, minimizing net heat loss from the lesion site. Jain and Wolf (37) found that lesion size was best predicted by titrating the delivered power to maintain a constant electrode tip temperature and thus a constant temperature gradient and lesion size. Cheng et al. (22) discarded the perfusion term from the bio-heat equation in their study of RF thermal ablation on the basis that the similarity between lesions induced in saline-gel and perfused liver reflected the vascular homogeneity of the ablated portion of liver and its distance from large vessels. The assumption is that the volume of tissue ablated in certain clinical applications is small and contained within the capillary network where the blood flow is slow and has negligible effect during the few minutes of hyperthermic application (22).

Thus, while PVA-C is only able to record peak temperature and not a full thermal history, the extent of the heat-affected region characterized by the isothermal surfaces at the equivalent model values of 43°C and 45°C may be described by using PVA-C. This modeling could provide useful information about the shape of lesions produced in tissue by RF probes with constant tip temperatures, since the research cited above has shown tip temperature to be the best predictor of lesion size. In particular, the shape of the lesion produced by a nonstandard probe (e.g., designed to create a conformal lesion) could be readily determined. Note that the critical temperatures of tissue may not be directly modeled in PVA-C due to the differences in electrical and thermal conductivity constants, but the extent of hyperthermic lesions produced in PVA-C may be related to tissue or to theoretical models through known relationships.

CONCLUSION

PVA-C exhibits a temperature memory when temporarily heated from ambient to a temperature between 45–70°C. This ability to record temperature is affected by the concentration, number of FTCs, and thaw rates of the PVA-C, due to their effects on the degree of cross-linking that initially occurs during cryogel formation. The temperature memory is demonstrated by a positive, approximately linear, relationship between both the T_1 and T_2 relaxation

times and increasing temperature, with the most effective temperature range being 45–70°C. We suggest that 10% 2FTC PVA-C is the best candidate, particularly when analyzing with T_1 , because of its linearity of scale, its repeatability, its accuracy and the slope of the relaxation time to temperature curve.

The relationship between PVA-C and temperature is used to create a dependence scale which relates T_1 or T_2 values to specific temperatures. A standardized scale may be used to determine an unknown temperature or heat distribution in a sample of 10% 2FTC PVA-C, with an error of 0.8°C, by matching T_1 values to corresponding temperatures.

The possible extension of this temperature mapping method to modeling the shape of lesions created by a heat source in tissue requires consideration of the complex response of tissue to a thermal history. Although results indicate that PVA-C does not record thermal history, it does record peak temperatures and may be a useful indicator of lesions characterized by the isothermal surface of 45°C, created by standard or nonstandard RF probes with constant tip temperatures. This may be particularly useful in designing new probes that can produce conformal lesions in tissue. Differences in thermal and electrical conductivities must be included in a tissue-mimicking model. Future work will include applying the temperature scales in 3D hyperthermic heating studies to analyze a volumetric heating pattern produced by RF probes, focused ultrasound, or radio-diathermy.

ACKNOWLEDGMENTS

The authors thank Dr. K.C. Chu, Dr. B.K. Rutt, Dr. I. MacDonald, S. Deoni, and K. Onu for assistance.

REFERENCES

- Chu KC, Jordan KJ, Battista JJ, VanDyk J, Rutt BK. PVA-Fricke hydrogel and cryogel: Two new gel dosimetry systems with low Fe^{3+} diffusion. *Phys Med Biol* 2000;45:955–969.
- Low DA, Dempsey JF, Venkatesan R, Mitic S, Markman J, Haacke EM, Purdy JA. Evaluation of polymer gels and MRI as a 3-D dosimeter for intensity-modulated radiation therapy. *Med Phys* 1999;26:1542–1551.
- Pappas E, Maris T, Angelopoulos A, Paparigopoulou M, Sakelliou L, Sandilos P, Voyiatzi S, Vlachos L. A new polymer gel for magnetic resonance imaging (MRI) radiation dosimetry. *Phys Med Biol* 1999;44:2677–2684.
- DeDeene Y, DeWagter C, VanDuyse B, Derycke S, Mersseman B, DeGerssem W, Voet T, Achten E, DeNeve W. Validation of MR-based polymer gel dosimetry as a preclinical three-dimensional verification tool in conformal radiotherapy. *Magn Reson Med* 2000;43:116–125.
- Gambarini G, Monti D, Fumagalli ML, Birattari C, Salvadori P. Phantom dosimeters examined by NMR analysis: a promising technique for 3-D determination of absorbed dose. *Appl Radiat Isot* 1997;48:1477–1484.
- Cosman ER. Radiofrequency lesions. In: Gildenberg PL, Tasker RR, editors. *Textbook of stereotactic and functional neurosurgery*. New York: McGraw-Hill; 1998. p 973–985.
- Diederich CJ, Hynynen K. Ultrasound technology for hyperthermia. *Ultrasound Med Biol* 1999;25:871–887.
- Skinner MG, Iizuka MN, Kolios MC, Sherar MD. A theoretical comparison of energy sources—microwave, ultrasound and laser—for interstitial thermal therapy. *Phys Med Biol* 1998;43:3535–3547.
- Peters RD, Hinks RS, Henkelman RM. Ex vivo tissue-type independence in proton-resonance frequency shift in MR thermometry. *Magn Reson Med* 1998;40:454–459.
- Shamberger RC, Talbot TL, Tipton HW, Thibault LE, Brennan MF. The effect of ultrasonic and thermal treatment on wounds. *Plast Reconstr Surg* 1981;68:860–870.
- Fan M, Ascher PW, Schrottner O, Ebner F, Germann RH, Kleinert R. Interstitial 1.06 Nd:YAG laser thermotherapy for brain tumors under real-time monitoring of MRI: experimental study and phase I clinical trial. *J Clin Laser Med Surg* 1992;10:355–361.
- Chung AN, Jolesz FA, Hynynen K. Thermal dosimetry of a focused ultrasound beam in vivo by magnetic resonance imaging. *Med Phys* 1999;26:2017–2026.
- Le Bihan D, Delannoy J, Levin RL. Temperature mapping with MR imaging of molecular diffusion: application to hyperthermia. *Radiology* 1989;171:853–857.
- Dickinson RJ, Hall AS, Hind AJ, Young IR. Measurement of changes in tissue temperature using MR imaging. *J Comput Assist Tomogr* 1986;10:468–472.
- Cline HE, Hynynen K, Hardy CJ, Watkins RD, Schenck JF, Jolesz FA. MR temperature mapping of focused ultrasound surgery. *Magn Reson Med* 1994;31:628–636.
- Graham SJ, Stanisz GJ, Kecojevic A, Bronskill MJ, Henkelman RM. Analysis of changes in MR properties of tissues after heat treatment. *Magn Reson Med* 1999;42:1061–1071.
- Parker DL, Smith V, Sheldon P, Crooks LE, Fussell L. Temperature distribution measurements in two-dimensional MR imaging. *Med Phys* 1983;10:321–325.
- Peters RD, Hinks RS, Henkelman RM. Heat-source orientation and geometry dependence in proton-resonance frequency shift magnetic resonance thermometry. *Magn Reson Med* 1999;41:909–918.
- Wang Y, Plewes DB. An MRI calorimetry technique to measure tissue ultrasound absorption. *Magn Reson Med* 1999;42:158–166.
- Young IR, Hand JW, Oatridge A, Prior MV. Modeling and observation of temperature changes in vivo using MRI. *Magn Reson Med* 1994;32:358–369.
- de Zwart JA, Vimeux FC, Delalande C, Canioni P, Moonen CT. Fast lipid-suppressed MR temperature mapping with echo-shifted gradient-echo imaging and spectral-spatial excitation. *Magn Reson Med* 1999;42:53–59.
- Cheng Y-CN, Brown RW, Chung Y-C, Duerk JL, Fujita H, Lewin JS, Schuele DE, Shvartsman S. Calculated RF electric field and temperature distributions in RF thermal ablation: comparison with gel experiments and liver imaging. *J Magn Reson Imaging* 1998;8:70–76.
- Surry KJM, Blake CC, Chu KC, Gordon M, Rutt BK, Fenster A, Peters TM. Poly(vinyl alcohol) phantoms for use in MR and US imaging. *Med Phys* 1998;25:1082.
- Chu KC, Rutt BK. Poly(vinyl alcohol) cryogel: an ideal phantom material for MR studies of arterial flow and elasticity. *Magn Reson Med* 1997;37:314–319.
- Dyson RW. *Specialty polymers*, 2nd ed. London: Blackie Academic and Professional; 1998. p 32–33, 78–85.
- Mano I, Goshima H, Nambu M, Iio M. New poly(vinyl alcohol) gel material for MRI phantoms. *Magn Reson Med* 1986;3:921–926.
- Nagura M, Hamano T, Ishikawa H. Structures of poly(vinyl alcohol) hydrogel prepared by repeated freezing and melting. *Polymer* 1989;30:762–765.
- Mori Y, Tokura H, Yoshikawa M. Properties of hydrogels synthesized by freezing and thawing aqueous poly(vinyl alcohol) solutions and their applications. *J Mater Sci* 1997;32:491–496.
- Touloukian YS, Powell RW, Ho CY, Klemens PG. *Thermal conductivity: nonmetallic solids, thermophysical properties of matter*, vol. 2. New York: IFI/Plenum; 1970. p 17a–18a.
- Bennett CO, Myers JE. *Momentum heat and transfer*, 3rd ed. Carberry JJ, Fair JR, Peters MS, Schowalter WR, Wei J, editors. McGraw-Hill Chemical Engineering Series. New York: McGraw-Hill; 1982. p 249–273.
- Field SB. In vivo aspects of hyperthermic oncology. In: Field SB, Hand JW, editors. *An introduction to the practical aspects of clinical hyperthermia*. London: Taylor and Francis; 1990. p 55–68.
- Field SB, Raaphorst GP. Thermal dose. In: Field SB, Hand JW, editors. *An introduction to the practical aspects of clinical hyperthermia*. London: Taylor and Francis; 1990. p 69–76.
- Henle KJ. *Thermotolerance. Thermotolerance and thermophily*, vol. 1. Boca Raton, FL: CRC Press; 1987. p 73–93.
- Sminia P, Van Der Zee J, Wondergem J, Haveman J. Effect of hyperthermia on the central nervous system: a review. *Int J Hyperthermia* 1994;10:1–30.
- Urano M. Kinetics of thermotolerance in normal and tumor tissues: a review. *Cancer Res* 1986;46:474–482.
- Lagendijk JWW. Hyperthermia treatment planning. *Phys Med Biol* 2000;45:R61–R76.

37. Jain MK, Wolf PD. Temperature-controlled and constant-power radio-frequency ablation: what affects lesion growth? *IEEE Trans Biomed Eng* 1999;46:1405–1412.
38. Haines DE, Watson DD. Tissue heating during radiofrequency catheter ablation: a thermodynamic model and observations in isolated perfused and superfused canine right ventricular free wall. *Pacing Clin Electrophysiol* 1989;12:962–976.
39. Labonte S. Numerical model for radio-frequency ablation of the endocardium and its experimental validation. *IEEE Trans Biomed Eng* 1994;41:108–115.
40. Shahidi AV, Savard P. A finite element model for radiofrequency ablation of the myocardium. *IEEE Trans Biomed Eng* 1994;41:963–968.
41. Panescu D, Wayne JG, Fleischman SD, Miroznik MS, Swanson DK, Webster JG. Three-dimensional finite element analysis of current density and temperature distributions during radio-frequency ablation. *IEEE Trans Biomed Eng* 1995;42:879–890.
42. Ho CY, Powell RW, Liley PE. Thermal conductivity of the elements: a comprehensive review. *J Phys Chem Ref Data* 1974;3(Suppl 1):1–38. American Institute of Physics and the American Chemical Society, New York, 1975.
43. Molloy JA, Ritter RC, Broaddus WC, Grady MS, Howard MA 3d, Quate EG, Gillies GT. Thermodynamics of movable inductively heated seeds for the treatment of brain tumors. *Med Phys* 1991;18:794–803.